Acoust. Sci. & Tech. **39**, 6 (2018)

PAPER

Impedance modeling of elastic boundary support in the vibration field of a thin plate

Naohisa Inoue* and Tetsuya Sakuma†

Graduate School of Frontier Sciences, The University of Tokyo, Environ. Bldg., 5–1–5 Kashiwanoha, Kashiwa, 277–8563 Japan

(*Received 1 March 2018, Accepted for publication 17 July 2018*)

Abstract: Modeling of elastic boundary support is crucial for simulating realistic vibro-acoustical behaviors of plate-like structures. In this paper, the mechanical and moment impedances of an elastic support material are derived in closed form under several assumptions, and three basic studies are conducted on a vibration system of a thin plate supported with an elastic material. First, bending wave reflection from the impedance boundary is theoretically analyzed to clarify the incidence angle dependence of vibration energy absorption coefficient. Second, the proposed impedance model is validated in comparison with the precise finite element model of the elastic support material. Finally, as an application of the impedance model, loss factor measurement is numerically modeled, which reveals that the calculated loss factors are generally greater than the theoretical values for the diffuse vibration field.

Keywords: Thin plate, Elastic support condition, Mechanical impedance, Moment impedance, Finite element method, Loss factor

PACS number: 43.40.Dx, 43.40.Tm, 43.55.Wk [doi:10.1250/ast.39.387]

1. INTRODUCTION

Understanding vibro-acoustical behaviors of plate-like structures is of great interest in many fields of noise control engineering. Regarding the acoustic radiation from a rectangular plate, Berry *et al.* have made a significant remark that the radiation mechanism strongly depends on the boundary condition of the plate [1]. In the paper, modal radiation efficiencies were provided for the plate with arbitrary combinations of four kinds of ideal boundary condition. However, plates are usually supported by elastic materials, where the actual condition on their joining face is an intermediate state among the ideal conditions. Another important aspect is that energy loss occurs in the reflection of bending waves at the elastic supported edges, which reduces the radiation from modal vibrations of the plate [2]. This is also directly related to the airborne sound insulation performance. Thus, modeling of the elastic boundary support is crucial for simulating realistic vibro-acoustical behaviors of plate-like structures.

The elastic boundary support has been usually modeled with mechanical and moment impedances, but it is not yet well established how to determine the impedances. Several papers have dedicated to investigate the effect of translational and rotational restraint on natural frequencies of finite plates [3–7], where the analysis was performed with assuming lumped constants of stiffness, inertance and resistance for the impedance boundary condition. However, it is not clear to what extent this lumped model is applicable, especially, in relation to the size of an elastic support material and the frequency. Besides, input parameters of the boundary impedances are often experimentally determined by excitation tests. The total loss factor (TLF) measurement by reverberation method is one of the most common measurement [8]. However, the measured value has not been investigated in terms of the discrepancy from the theoretical value.

Focusing on a thin plate supported by an elastic material with rectangular cross section, this paper is dedicated to improve the usability of the impedance boundary modeling. In Sect. 2, closed-form expressions of equivalent mechanical and moment impedances are derived under several assumptions. Then, theoretical analysis is provided to investigate the behaviors of bending wave absorption at the impedance boundary. In Sect. 3, finite element analysis is conducted to clarify the reliable condition of impedance boundary modeling. The result by

*e-mail: n-inoue@edu.k.u-tokyo.ac.jp
†e-mail: sakuma@k.u-tokyo.ac.jp

proposed impedance model are compared with those by the precise model. Assuming the experimental determination of the input value for the impedance model, a measurement of TLF is numerically simulated by using the impedance model in Sect. 4. The behavior of TLF calculated for a finite plate is examined in comparison with the theoretical values for the diffuse field.

2. THEORETICAL ANALYSIS

2.1. Governing Equation

A flat plate is assumed to lie on the x-y plane of the Cartesian coordinate. $e^{j\omega t}$ is assumed as the time convention throughout this paper. The time-harmonic equation of the Kirchhoff-Love thin plate vibration theory is given as

$$B\nabla^2\nabla^2 w - \rho_p\omega^2 w = f_z + z\frac{\partial f_x}{\partial x} + z\frac{\partial f_y}{\partial y}, \tag{1}$$

where ∇^2 is the Laplace operator, w is the out-of-plane displacement, B and ρ_p are the flexural rigidity and the area density of the plate. B is given by $B = E_p {t_p}^3/[12(1-\nu^2)]$, where E_p, ν and t_p are the Young's modulus, the Poisson's ratio and the thickness of the plate, respectively. f_x, f_y and f_z are the external stress acting on the plate surface in each direction. z is the signed distance from the mid-plane of the plate, which is $t_p/2$ on the upper face and $-t_p/2$ on the bottom face, respectively. The relation between the bending–torsional moments and the displacement is described as follows.

$$M_{\alpha\beta} = -B\left[(1-\nu)\frac{\partial^2 w}{\partial\alpha\partial\beta} + \delta_{\alpha,\beta}\nu\nabla^2 w\right], \tag{2}$$

where α and β take x or y. $\delta_{\alpha,\beta}$ is the component of the unit tensor. Throughout this paper, the internal loss factor of the plate, η_p, is set as zero in order to focus on the effect of the edge damping.

2.2. Impedance Boundary Conditions

As Eq. (1) is the partial differential equation of fourth order, two conditions should be defined at a boundary: one is for translational motion and the other is for rotational motion. Assuming the local reactive boundary, these conditions can be generally described by using the mechanical and moment impedances, Z_Q and Z_M, as follows.

$$\tilde{Q} = \left(\frac{\partial M_n}{\partial n} + 2\frac{\partial M_s}{\partial s}\right) = -j\omega Z_Q w, \tag{3}$$

$$M_n = j\omega Z_M \frac{\partial w}{\partial n}, \tag{4}$$

where $\tilde{Q}$, M_n, and M_s are the effective shear force, normal and torsional moments along the boundary, respectively. $\partial/\partial n$ and $\partial/\partial s$ are the normal and tangential directional derivative along the plate's boundary, respectively.

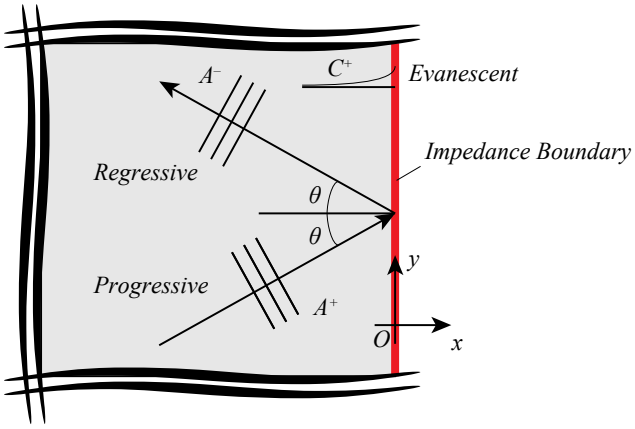

Fig. 1 Problem setting for the analysis of the bending wave reflection from the impedance boundary.

2.3. Oblique-incidence Reflection Coefficient

As depicted in Fig. 1, let us consider a situation where the plane propagative bending wave impinges to the boundary of $x = 0$ at an incidence angle of θ. In this semi-near field, general solution of the Eq. (1) is given as [9]

$$w(x,y) = (A^+ e^{-jk_{Bx}x} + A^- e^{jk_{Bx}x} + C^+ e^{k_{Ex}x})e^{-jk_{By}y}, \tag{5}$$

where $k_{Bx} = k_B\cos\theta$, $k_{By} = k_B\sin\theta$ and $k_{Ex} = k_B(1+\sin^2\theta)^{1/2}$. k_B is the bending wave number on the plate defined as $k_B = \omega^{1/2}(B/\rho_p)^{1/4}$. Substituting Eqs. (2) and (5) into Eq. (3), the following relation is obtained.

$$(\gamma_-\beta_+ - z_q)A^+ - (\gamma_-\beta_+ + z_q)A^- - (j\gamma_+\beta_- + z_q)C^+ = 0, \tag{6}$$

where z_q is the normalized mechanical impedance defined as $z_q = \omega Z_Q/({k_B}^3 B)$. And the following values are introduced, $\beta_\pm = 1 \pm (1-\nu)\sin^2\theta$ and $\gamma_\pm = (1 \pm \sin^2\theta)^{1/2}$. In the same way, substituting Eqs. (2) and (5) into Eq. (4), the following relation is obtained.

$$(\beta_- - z_m\gamma_-)A^+ + (\beta_- + z_m\gamma_-)A^- - (\beta_+ + jz_m\gamma_+)C^+ = 0, \tag{7}$$

where z_m is the normalized moment impedance defined as $z_m = \omega Z_M/(k_B B)$.

Combining Eqs. (6) and (7), the oblique-incidence reflection coefficient is obtained as

$$r(\theta) = \frac{A^-}{A^+} = \frac{\left(\begin{array}{l}\gamma_-\beta_+^2 - 2z_q + \gamma_- z_q z_m \\ \quad - j\gamma_+(\beta_-^2 + z_q z_m - 2\gamma_- z_m)\end{array}\right)}{\left(\begin{array}{l}\gamma_-\beta_+^2 + 2z_q + \gamma_- z_q z_m \\ \quad + j\gamma_+(\beta_-^2 + z_q z_m + 2\gamma_- z_m)\end{array}\right)}. \tag{8}$$

Furthermore, oblique-incidence vibration absorption coefficient is given as $\alpha(\theta) = 1 - |r(\theta)|^2$.

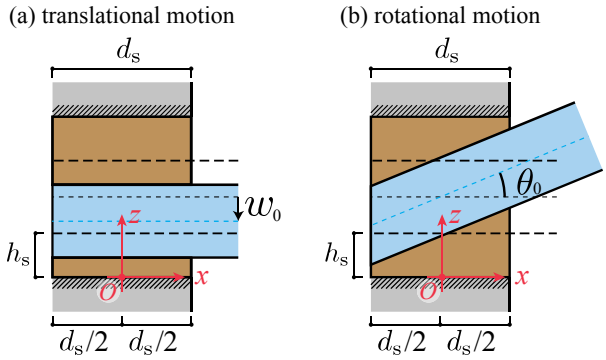

Fig. 2 Assumed deformations of a rectangular support material for (a) translational and (b) rotational motions.

2.4. Equivalent Impedances of a Rectangular Elastic Support Material

Let us consider deformations of a rectangular elastic support material as depicted in Fig. 2. The three-dimensional displacements of the support material are continuous to those of the plate on the joining face and fixed at the opposite face. Furthermore, the other faces are under the free support. In order to derive the impedances in the closed form, the following assumptions are introduced:

1. only the one-dimensional longitudinal vibration is excited in the thickness direction of the support material,
2. the translational out-of-plane displacement and the rotational slope of the plate are uniform over the supporting depth.

The validity of the first assumptions is numerically investigated in Sect. 3. The second assumption is considered to be valid when the bending wavelength is sufficiently larger than the supporting depth.

Under the first assumption, the longitudinal modal stress in the support material of the lower side is expressed as

$$\sigma_z(x,z) = k_1 \tilde{E}_s w(x) \frac{\cos(k_1 z)}{\sin(k_1 h_s)}, \tag{9}$$

where $w(x)$ is the displacement on the joining face. The second assumption states that the displacement is $w(x) = w_0 + \theta_0 x$ with the constant translational displacement w_0 and the constant rotational slope θ_0. h_s is the thickness of the support material, k_l is the wave number of the longitudinal wave in the support material, and $\tilde{E}_s$ is the complex Young's modulus defined as $\tilde{E}_s = E_s(1 + j\eta_s)$ with the loss factor η_s. For the translational motion, the force on the joining face, $z = h_s$, is obtained by integrating $\sigma(x, h_s)$ over the supporting depth d_s. Considering the reaction forces of the support materials on both sides, the mechanical impedance is obtained as follows.

$$Z_Q = \frac{2\int_{-d_s/2}^{d_s/2} \sigma_z(x,h_s)dx}{j\omega w_0} = \frac{2\rho_s \tilde{c}_1 d_s}{j\tan(\omega h_s/\tilde{c}_1)} \tag{10}$$

where $\tilde{c}_1$ is the speed of longitudinal wave defined as $\tilde{c}_1 = (\tilde{E}_s/\rho_s)^{1/2}$ and ρ_s is the material density of the support material. For the rotational motion, the moment on the joining face is obtained by integrating $\sigma(x, h_s) \times x$ over the supporting depth. Considering the reaction moments of both sides, the moment impedance is obtained as follows.

$$Z_M = \frac{2\int_{-d_s/2}^{d_s/2} \sigma_z(x,h_s)xdx}{j\omega\theta_0} = \frac{\rho_s \tilde{c}_1 d_s^3}{6j\tan(\omega h_s/\tilde{c}_1)} \tag{11}$$

2.5. Discussions

Vibrational absorption coefficient of the support material is investigated according to the above-described theory and model.

2.5.1. Resonance frequencies

Absorbing mechanisms can be divided into two classes: one is the global mass-spring resonance composed of the plate (mass) and the support material (spring), and the other is local modal vibration of the support material.

First, let us consider the global resonance system in the low frequency range where $\omega h_s/\tilde{c}_1 \ll \pi/2$. In the case, the normalized mechanical and moment impedances of Eqs. (10) and (11) are reduced to

$$z_q = \hat{z}_q(\eta_s - j), \quad \hat{z}_q = \frac{2E_s d_s}{Bk_B^3 h_s}, \tag{12}$$

$$z_m = \hat{z}_m(\eta_s - j), \quad \hat{z}_m = \frac{E_s d_s^3}{6Bk_B h_s}, \tag{13}$$

respectively. The inertial effect of the support material is neglected through this approximation. Substituting Eqs. (12) and (13) and $\theta = 0$ into Eq. (8), normal-incidence vibration absorption coefficient is obtained as

$$\alpha_n = \frac{4(\eta\hat{z}_m\hat{z}_q^2 + \eta^2\hat{z}_m^2\hat{z}_q + \hat{z}_m^2\hat{z}_q + 2\hat{z}_m\hat{z}_q + \hat{z}_q + \eta\hat{z}_m)}{\left(\begin{array}{r} 2[(\eta^2+1)\hat{z}_m^2 + (\eta+1)\hat{z}_m + 1](\hat{z}_q^2 + \hat{z}_q + 1) \\ -\eta^2\hat{z}_m^2\hat{z}_q^2 - (\hat{z}_m\hat{z}_q - 1)^2 \end{array}\right)}. \tag{14}$$

When the normalized moment impedance is fixed to extreme value, zero or infinity, the translational mass-spring resonance frequency, f_q, at which Eq. (14) becomes max leads

$$f_q = \frac{1}{2\pi}\sqrt{\frac{B}{\rho_p}\left[c_M(1+\eta_s^2)\left(\frac{2E_s d_s}{Bh_s}\right)^2\right]^{\frac{1}{3}}}, \tag{15}$$

where $c_M = 2$ for $z_M = 0$ and $c_M = 1/2$ for $z_M = \infty$. Similarly, when the normalized mechanical impedance is fixed to zero or infinity, the rotational mass-spring

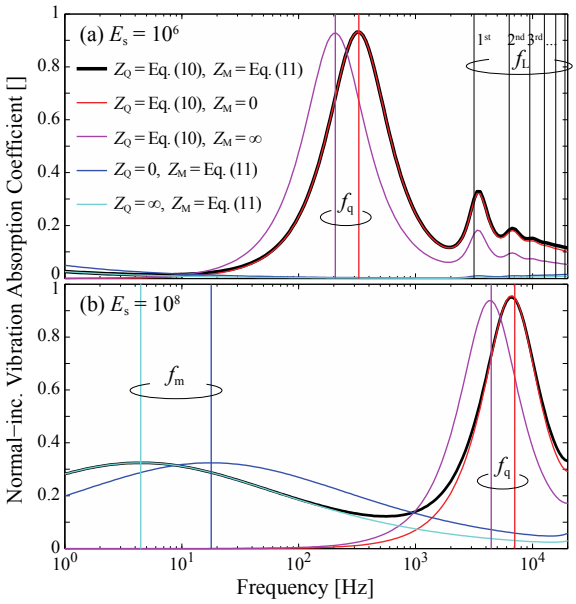

Fig. 3 Normal-incidence vibration absorption coefficient calculated with changing Young's modulus of the support material: (a) 10^6 and (b) 10^8.

resonance frequency, f_m, at which Eq. (14) becomes max leads

$$f_m = \frac{1}{2\pi}\sqrt{\frac{B}{\rho_p}}c_Q(1+\eta_s^2)\left(\frac{E_s d_s^3}{6Bh_s}\right)^2, \qquad (16)$$

where $c_Q = 2$ for $Z_Q = 0$ and $c_Q = 1/2$ for $Z_Q = \infty$. For a solid cross-section plate, $f_q \propto 1/t_p$ and $f_m \propto 1/t_p^5$. Accordingly, the rotational mass-spring resonance frequency is strongly dependent on the plate thickness as well as the supporting depth.

Second, the n-th modal resonance of the support material occurs around

$$f_L = \frac{n}{2h_s}\sqrt{\frac{E_s}{\rho_s}}.$$

Both Z_Q and Z_M approach infinity around f_L, which means the boundary condition becomes the clamped support. Furthermore, there are the frequencies at which both Z_Q and Z_M approach zero, and the free support condition arises.

2.5.2. Normal-incidence vibration absorption coefficient

Figure 3 shows the normal-incidence vibration absorption coefficient, α_n, calculated for the glass plate and supporting putty. In addition, either Z_Q or Z_M is set to zero or infinity, and four combinations of Z_Q and Z_M are shown as references. The physical properties for the calculation are listed in Table 1.

In theory, the vibrational behavior of a mass-spring system switches from stiffness control to mass control at the resonance frequency. Then, in the present case where $f_m < f_q$, the cyan ($Z_Q = \infty$) and red ($Z_M = 0$) lines give good approximation to the black thick line around f_m and

Table 1 Physical properties of the plate and supporting material.

property	plate	support
	Glass	Putty
Young's modulus [N/m^2]	$E_p = 7.5 \times 10^{10}$	$E_s = 1.0 \times 10^6, 1.0 \times 10^8$
Poisson's ratio [ ]	$\nu = 0.22$	N/A
Loss Factor [ ]	$\eta_p = 0$	$\eta_s = 0.5$
Material Density [kg/m^3]	$\rho_p/t_p = 2{,}500$	$\rho_s = 1{,}000$
Thickness [m]	$t_p = 0.01$	$h_s = 0.005$
Depth [m]	N/A	$d_s = 0.015$

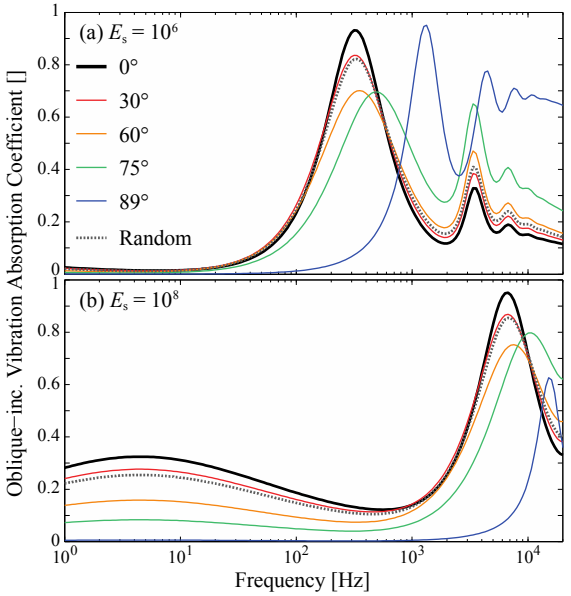

Fig. 4 Oblique- and random-incidence vibration absorption coefficient calculated with changing Young's modulus of the support material: (a) 10^6 and (b) 10^8.

f_q, respectively. The result implies that the support condition is an intermediate state between simple and clamped supports around f_m and between simple and free supports around f_q. Moreover, the translational mass-spring resonance of the black line appears at slightly lower frequency than f_q. This is because Eq. (15) is derived by neglecting the inertial effect of the support material. Nevertheless, the global resonance frequencies can be estimated fairly well by Eqs. (15) and (16).

In the modal resonance frequency range, the translational motion contributes to the energy absorption dominantly because α_n calculated for the lossless Z_Q are considerably small. As the rotational constraint become stronger, absorption due to the longitudinal-mode resonance decreases.

2.5.3. Oblique- and random-incidence vibration absorption coefficient

Figure 4 shows the oblique-incidence vibration absorption coefficients, $\alpha(\theta)$, calculated for the same plate and support material. In the incidence angle of 30 and 60

degrees, absorption due to the global resonances decreases, whereas absorption due to the modal resonance increases. Furthermore, the resonance frequencies in oblique-incidence appear around at that of the normal incidence. Above the incidence angle of 60 degree, the translational mass-spring resonance frequencies are shifted to higher frequency range, and the absorption peak due to the rotational mass-spring resonance fades into zero.

Figure 4 also shows the random-incidence vibration absorption coefficients, α_r, calculated for the same plate and support material by the following statistical average based on the two-dimensional diffuse field assumption,

$$\alpha_r = \frac{1}{2}\int_{-\pi/2}^{\pi/2} \alpha(\theta)\cos\theta d\theta. \tag{17}$$

It is obvious from Eq. (17) that values around the normal-incidence dominantly contribute to the statistical average one. Then the frequency characteristics of α_r show almost the same tendency as those of normal-incidence. Besides, the $\alpha(\theta)$ at 30 degree approximates α_r well in quantity, and this relation moderately holds for other physical parameters of the plate and support material. This tendency may be practically useful for experimental estimation of the lamped constants of the boundary impedances or the physical parameters of the support material. Because, in the estimation procedure, measured α_r can be directly compared with the theoretical $\alpha(\theta)$ at 30 degree obtained by Eq. (8).

3. NUMERICAL INVESTIGATION

This section discusses the validity of the mechanical and moment impedances given in the previous section through the finite element analysis (FEA). Figure 5 shows the problem setting and the domain notation in this section. The boundary condition of the plate and the elastic material is free support unless otherwise indicated.

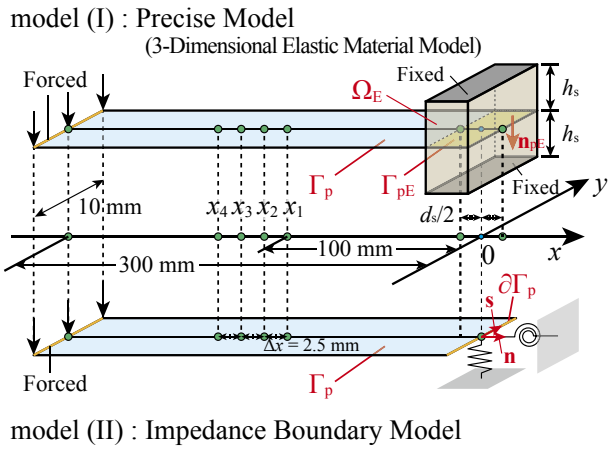

Fig. 5 Problem settings and domain notation for calculating mechanical and moment impedances and vibration absorption coefficient.

3.1. Weak Formulation for the Finite Element Analysis

In the following, an analysis theory of coupled vibration fields of a plate and a three-dimensional elastic body is formulated.

First, the weak form of Eq. (1) is expressed as

$$\int_{\Gamma_p+\Gamma_{pE}} \left(\sum_{\alpha,\beta=x,y} \frac{\partial^2 \delta w}{\partial\alpha\partial\beta} M_{\alpha\beta} - \rho_p \omega^2 \delta w w \right) dS + \int_{\partial\Gamma_p} \left[\frac{\partial \delta w}{\partial n} M_n - \delta w \left(\frac{\partial M_n}{\partial n} + 2\frac{\partial M_s}{\partial s} \right) \right] dL + \int_{\Gamma_{pE}} \left[-\delta w f_z + z \sum_{\alpha=x,y} \left(\frac{\partial \delta w}{\partial \alpha} f_\alpha \right) \right] dS = 0, \tag{18}$$

where δw is the admissible variation of the out-of-plane displacement. It is noted that the work done by the corner force is neglected in Eq. (18). The contour integral terms along $\partial\Gamma_p$ represent the works done by the elastic support, and are rewritten with Eqs. (3) and (4) as

$$\int_{\partial\Gamma_p} \left[\frac{\partial \delta w}{\partial n} M_n - \delta w \left(\frac{\partial M_n}{\partial n} + 2\frac{\partial M_s}{\partial s} \right) \right] dL = j\omega \int_{\partial\Gamma_p} \left(\frac{\partial \delta w}{\partial n} Z_M \frac{\partial w}{\partial n} + \delta w Z_Q w \right) dL.$$

Z_Q and Z_M are evaluated by Eqs. (10) and (11), respectively. The surface integral terms in the third line of Eq. (18) represent the work done by external forces. In this paper, the ACM quadrangle element is used for the discretization and interpolation.

Second, the vibration field in the support material is analyzed according to the three-dimensional elastodynamic equation $\mathrm{div}\,\underline{\underline{\sigma}} + \rho_E \omega^2 \boldsymbol{u} = 0$ and the constitutive law $\underline{\underline{\sigma}} = \lambda\,\mathrm{div}\,\boldsymbol{u}\underline{\underline{1}} + 2\mu\underline{\underline{\varepsilon}}$, where $\boldsymbol{u}$ is the three-dimensional displacement vector, $\underline{\underline{\sigma}}$ and $\underline{\underline{\varepsilon}}$ are the stress and strain tensors, respectively, $\underline{\underline{1}}$ is the unit tensor, ρ_E is the material density, and λ and μ are the Lame's first and second coefficients, respectively. The weak form of the elastodynamic equation is given as

$$\int_{\Omega_E} (\delta\underline{\underline{\varepsilon}} : \underline{\underline{\sigma}} - \rho_E \omega^2 \delta\boldsymbol{u}\cdot\boldsymbol{u}) dV - \int_{\Gamma_{pE}} \delta\boldsymbol{u}\cdot(\underline{\underline{\sigma}}\cdot\boldsymbol{n}_{pE}) dS = 0, \tag{19}$$

where $\delta\boldsymbol{u}$ is the admissible variation of the three dimensional displacement, $\boldsymbol{n}_{pE}$ is the outward normal vector on the boundary Γ_{pE}. The surface integral term in the second line of Eq. (19) represents the work done by external forces. The 27-node 2nd-order hexahedral element is used for the discretization and interpolation.

Third, the continuity conditions on the interface Γ_{pE} between the elastic body and the plate vibration fields are given as

$$\begin{cases} -\underline{\underline{\sigma}} \cdot \boldsymbol{n}_{\mathrm{pE}} = \{f_x, f_y, f_z\} \\ \boldsymbol{u} = \left\{-z\dfrac{\partial w}{\partial x}, -z\dfrac{\partial w}{\partial y}, w\right\}. \end{cases} \tag{20}$$

The summation of the surface integral terms related to external forces in Eqs. (18) and (19) falls into zero under these conditions. This means that only the second equation of Eq. (20) is imposed explicitly by using common unknowns for nodal physical values in the finite element implementation.

3.2. Analysis Procedure of Normal-incidence Vibration Indicators

The bending vibration field becomes one-dimensional in the strip plate, which is described as

$$w(x) = A^{+}e^{-jk_{\mathrm{B}}x} + A^{-}e^{jk_{\mathrm{B}}x} + C^{+}e^{-k_{\mathrm{B}}x} + C^{-}e^{k_{\mathrm{B}}x}. \tag{21}$$

By observing the displacements at four points, x_1 to x_4, the following matrix equation can be set according to Eq. (21).

$$\begin{bmatrix} e^{-jk_{\mathrm{B}}x_1} & e^{jk_{\mathrm{B}}x_1} & e^{-k_{\mathrm{B}}x_1} & e^{k_{\mathrm{B}}x_1} \\ e^{-jk_{\mathrm{B}}x_2} & e^{jk_{\mathrm{B}}x_2} & e^{-k_{\mathrm{B}}x_2} & e^{k_{\mathrm{B}}x_2} \\ e^{-jk_{\mathrm{B}}x_3} & e^{jk_{\mathrm{B}}x_3} & e^{-k_{\mathrm{B}}x_3} & e^{k_{\mathrm{B}}x_3} \\ e^{-jk_{\mathrm{B}}x_4} & e^{jk_{\mathrm{B}}x_4} & e^{-k_{\mathrm{B}}x_4} & e^{k_{\mathrm{B}}x_4} \end{bmatrix} \begin{Bmatrix} A^{+} \\ A^{-} \\ C^{+} \\ C^{-} \end{Bmatrix} = \begin{Bmatrix} w(x_1) \\ w(x_2) \\ w(x_3) \\ w(x_4) \end{Bmatrix}$$

Then, the unknown amplitudes of propagative and evanescent waves, $\{\mathrm{A}^{+}, \mathrm{A}^{-}, \mathrm{C}^{+}, \mathrm{C}^{-}\}^{T}$, are obtained by solving the above equation. It was confirmed by a preliminary study that the theoretical impedances best approximate those of the precise model (I) just at the middle point of the joining depth: the middle point is set as $x = 0$ as depicted in Fig. 5. Then, normalized mechanical and moment impedances at $x = 0$ and normal-incidence vibration absorption coefficient are calculated as follows:

$$z'_{\mathrm{q}} = \frac{A^{+} - A^{-} + jC^{+} - jC^{-}}{A^{+} + A^{-} + C^{+} + C^{-}},$$

$$z'_{\mathrm{m}} = \frac{A^{+} + A^{-} - C^{+} - C^{-}}{A^{+} - A^{-} - jC^{+} + jC^{-}},$$

$$\alpha_{\mathrm{n}} = 1 - \left|\frac{A^{-}}{A^{+}}\right|^{2}.$$

3.3. Results and Discussions

FEA for the model (I) is performed under shear limp and elastic conditions for the support material. The former condition corresponds to the presented impedance model, and the shear stress is neglected in the FEA. The default physical properties are the same as those investigated in the previous section. Calculation is done at the 1/12 octave center frequency from 16 to 4,000 Hz. The wavelength of the bending wave on the plate at 4,000 Hz is 0.16 m, and enough larger than d_{s}. Then, the second assumption stated in Sect. 2.4 is acceptable in this point.

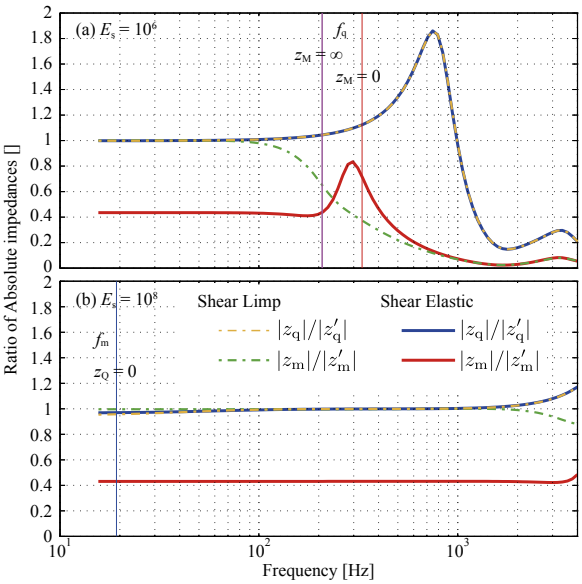

Fig. 6 Ratio of the absolute mechanical (moment) impedance of the model (II) to that of the theoretical model. The Young's moduli of the support material are (a) 10^6 and (b) 10^8.

Figure 6 shows calculation results: ratio of the absolute impedance of the model (II) to that of the model (I). For the shear limp condition, the theoretical model presented in Sect. 2 well approximates the mechanical and moment impedances around and below f_{q}. Above f_{q}, the support material can no longer be considered as a lumped constant system, which causes the pronounced discrepancy. Regarding the shear elastic model, the mechanical impedance is almost the same as those of the shear limp model. However, the moment impedance is underestimated in the entire frequency range by neglecting the shear stress of the support material. In particular, the ratio is constant below f_{q}. Note that these tendencies are also observed when changing plate thickness and the support material thickness and depth.

Figure 7 shows the calculation results of vibration absorption coefficient. Around and above f_{q}, shear limp and elastic models show almost the same value. Then the shear motion hardly contributes to the absorption. However, the rotational spring-mass resonance is shifted to higher frequency range by introducing the reaction to the shear motion. Furthermore, vibration absorption coefficients around and above the f_{q} in Fig. 7(a) approach those of the characteristics under the rigid moment impedance assumption ($z_{\mathrm{M}} = \infty$). These tendencies are the direct consequence of the underestimation of the moment impedance shown in Fig. 6.

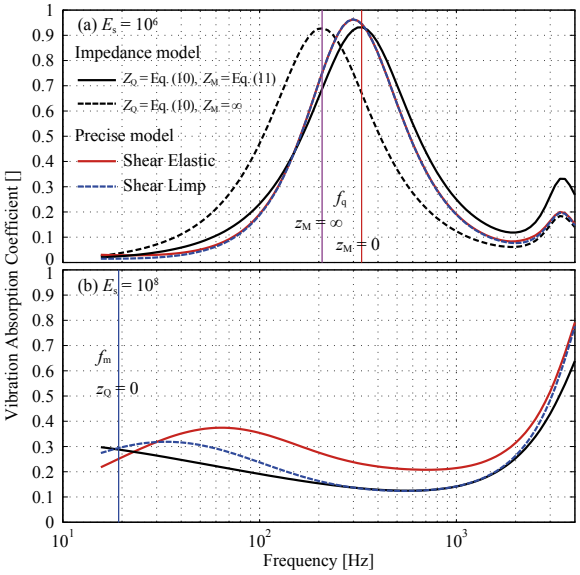

Fig. 7 Normal-incidence vibration absorption coefficient calculated for precise model (I). The Young's moduli of the support material are (a) 10^6 and (b) 10^8.

4. NUMERICAL MODELING OF A TOTAL LOSS FACTOR MEASUREMENT

The TLF measurement by the reverberation method is often performed to get or to estimate input values for theoretical or numerical calculations. However, it is not clear how measured values involve discrepancies from the theoretical values for the diffuse field, which increases the uncertainty of subsequent calculations. In this section, the TLF measurement is numerically modelled to understand the behavior of measured values. This practical information is valuable for experimental verification of the proposed impedance model in future work.

4.1. Theoretical Foundation

From the definition, the exponential decay rate, γ, of a system with a total loss factor η_{tot} is

$$\gamma = \eta_{\text{tot}}\omega. \tag{22}$$

Thus, when the 60 dB decay time, T_{60}, is measured, the total loss factor is obtained as

$$\eta_{\text{tot}} = \frac{6\ln 10}{\omega T_{60}}. \tag{23}$$

In the two-dimensional diffuse vibration field, the mean-free path is given as $\pi S/l_{\text{tot}}$ with the plate area S and the total perimeter length l_{tot}. Then the exponential decay rate, γ_{DF}, is

$$\gamma_{\text{DF}} = \frac{c_{\text{g}} l_{\text{tot}} \alpha_{\text{r}}}{\pi S}, \tag{24}$$

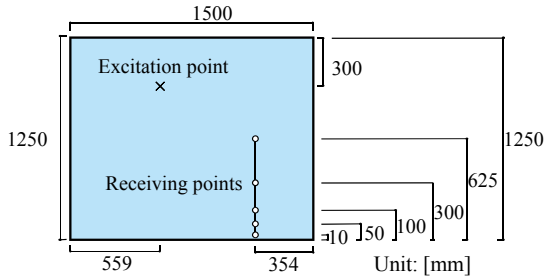

Fig. 8 A default geometry for the calculation of the total loss factor.

where c_{g} is the group velocity of the bending wave defined as $c_{\text{g}} = d\omega/dk_{\text{B}}$, and α_{r} is the vibration absorption coefficient for 2-D random-incidence. By comparing Eqs. (22) and (24), the total loss factor in the diffuse vibration field is given as

$$\eta_{\text{tot}} = \frac{c_{\text{g}} l_{\text{tot}} \alpha_{\text{r}}}{\pi\omega S}. \tag{25}$$

4.2. Numerical Analysis Conditions

Following the reference [10], calculation arrangement is set as illustrated in Fig. 8. In the FEA, all perimeters are set as impedance boundaries because this measurement is usually performed for specimens in normal service condition. The impedance values are given by Eqs. (10) and (11). Calculation is executed in 0.5 Hz intervals from 0 to 2,000 Hz. Subsequently, the transfer function of the acceleration response is converted to the transient response by the inverse Fourier transform. The reverberation time, T_{60}, is determined by the least square regression of the energy decay curve obtained by the backward integration of the filtered transient response. The total loss factor is determined by Eq. (23) and the 5-point-average of T_{60}.

4.3. Preliminary Study on the Band Analysis

It is well known that the reverberation of the band-pass filter (BPF) itself affects the reverberation time (RT) of the filtered response. In order to design the appropriate BPF, exponentially-decaying white noise (EDWN) is analyzed by using the FIR filters truncated by the hamming window. In order to approximately equalize the cut-off characteristics among the different bands, the order of the 1/3-octave band FIR filter of the center frequency f_{c} is set as $N \times 2^M$, where N is the order at 1 kHz and M is calculated by

$$M = \lfloor \log_2(f_{\text{c}}/1{,}000) + 0.5 \rfloor.$$

Changing the N and the decay rate of the EDWN, RTs of the filtered responses are calculated.

Figure 9 shows the relation between the RTs of BPFs and filtered EDWNs, where these RTs are normalized by

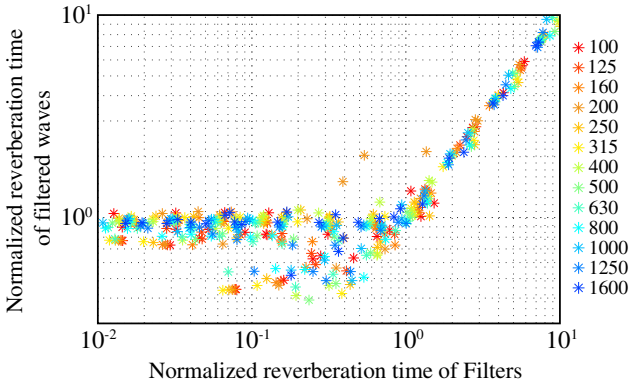

Fig. 9 Relation between the reverberation time of the FIR filters and filtered decay curves. Both RTs are normalized by the RT of the given exponential decay.

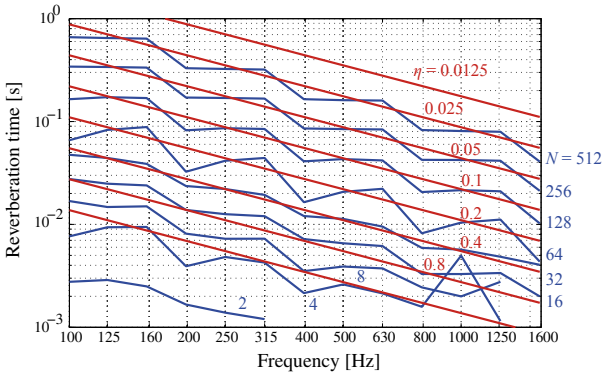

Fig. 10 Comparison between the reverberation times of the vibration system with a certain loss factor and the FIR filters with different orders.

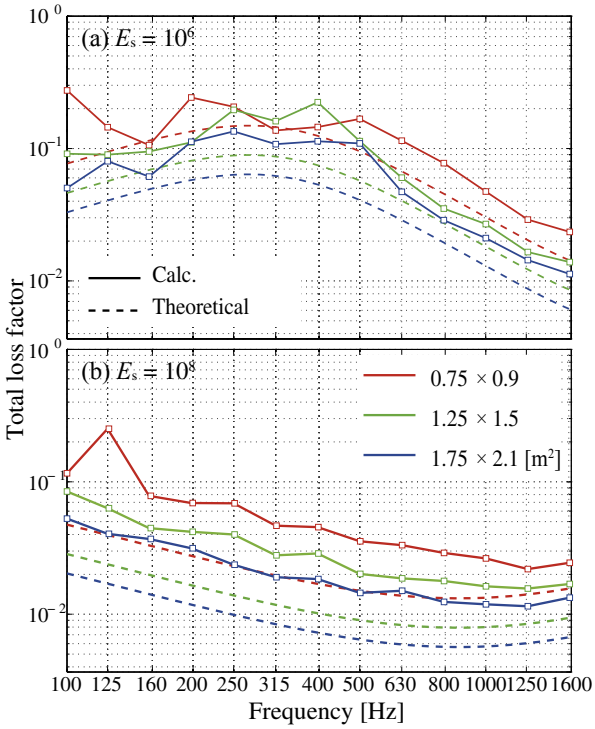

Fig. 11 Loss factors calculated for the plate with different sizes and the same aspect ratio. The Young's moduli of the support material are (a) 10^6 and (b) 10^8.

the decay rate given to the EDWN. This figure demonstrates that the RT of the BPF must be less than the RT of the target response. Figure 10 compares RT of a system with total loss factor η and that of the FIR-BPF with taps of $N \times 2^M$. In the following calculation, the theoretical total loss factor of a system is less than 0.2 at maximum. Then, the taps of the FIR filter are set as 64×2^M.

4.4. Results and Discussions

4.4.1. Effect of the plate size

It is obvious from Eq. (25) that TLF of a vibration system depends on the area and the total perimeter length. The TLF are calculated for three sizes of the plates: 40% smaller and larger plates than the default size.

Figure 11 compares calculated results with the theoretical values for the diffuse vibration field. The calculated results appear to capture the frequency trends of the theoretical values. Furthermore, TLFs for the smaller plate fluctuate more than those for larger plates do. However, the calculated values are two to four times larger than the theoretical values in the entire frequency range.

In general, the measurement of the sound absorption coefficient by reverberation room method involves two main error factors that cause the discrepancy from the theoretical value under the diffuse field assumption. One is the lack of the diffusivity. The diffuse field assumption becomes less effective to the rooms with parallel walls, and the grazing incidence to a boundary rarely arises. Then, non-diffuse effect usually appears as the underestimation of the sound absorption coefficient. The other is the diffraction at the edge of the finite specimen, which increase the effective incidence power. Then, the diffraction effect usually appears as the overestimation of the sound absorption coefficient. Similarly, the TLF measurement on the rectangular plate involves the non-diffuseness and the diffraction effects, and the latter seems to be predominant. Although all perimeters are impedance boundaries in the present study, the diffraction effect is considered to occur at the plate's corners. Besides, Fig. 9 demonstrates that the RT of the filtered response is determined more precisely when it is enough longer than the RT of a filter, which may also contribute to the overestimation. As a result, a large discrepancy can be seen in the frequency range at which the TLF is high.

4.4.2. Effect of the support material's properties

Figure 12(a) shows the calculated TLF with changing the support material's loss factor and fixing the Young's

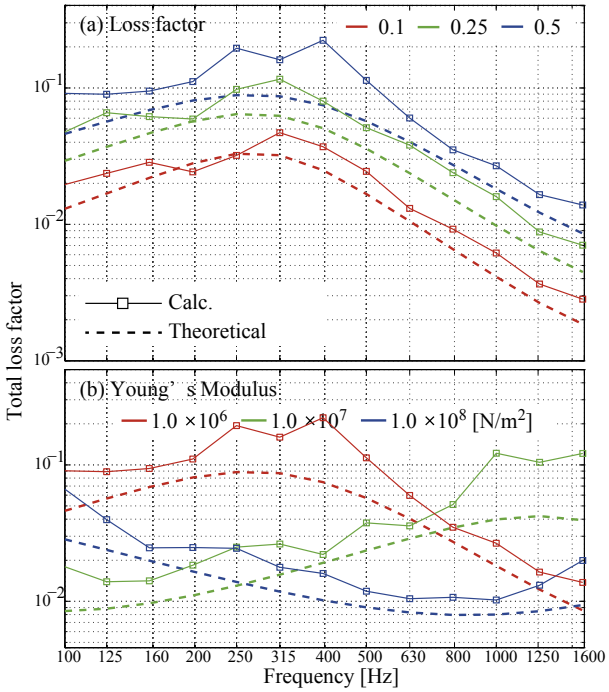

Fig. 12 Loss factors calculated with changing the physical property of the seal: (a) loss factor and (b) Young's modulus.

modulus to $1.0 \times 10^6\,\mathrm{N/m^2}$. Figure 12(b) shows the calculated TLF with changing the Young's modulus of the support material and fixing the loss factor to 0.5. As discussed in the above, the discrepancy between calculated and theoretical values appears to be large around the mass-spring resonance frequency at which the TLF becomes high.

Inverse estimation of the support material's physical parameters or equivalent resistance, stiffness and inertance constants is often performed in order to obtain the input parameters for theoretical and numerical calculations [11]. As noted in Sect. 2, the theoretical oblique-incidence vibration absorption coefficient at 30 degree can be used instead of random-incidence vibration absorption coefficient. However, from the above observations, the support material's damping parameter such as the loss factor and equivalent resistance constant can be overestimated.

5. CONCLUSION

In this paper, mechanical and moment impedances of a rectangular supporting elastic material were derived in closed form with the following assumptions:

1. only the one-dimensional longitudinal vibration is excited in the thickness direction of the support material,
2. the translational out-of-plane displacement and the rotational slope of the plate are uniform over the supporting depth.

Theoretical analysis was provided to investigate the behaviors of bending wave absorption at the impedance boundary. The translational and rotational mass-spring resonance systems are composed of the plate and the support material below the first longitudinal modal resonance frequency in the thickness direction of the support material. These resonance frequencies were also derived in the closed form. Furthermore, incidence angle dependency of the vibration absorption coefficient was confirmed to be weak until about 60-degree-incidence.

The proposed impedances were compared with those of the precise support material model by the finite element analysis. This study confirmed that the presented mechanical impedance agreed well with the precise model around and below the translational mass-spring resonance frequency. On the other hand, the presented moment impedance was underestimated in entire frequency range due to neglecting the shear reaction of the support material. Furthermore, above the translational mass-spring resonance frequency, the support material can no longer be replaced as a lumped constant system. Thus the impedance boundary model does not sufficiently simulate the behavior of the precise model in particular at high frequencies.

However, compared to the three dimensional elastic material model, the impedance boundary model can reduce the computational cost and the human effort to input calculation geometries. Furthermore, it is worth noting that numerical procedures employed in Sect. 3 can evaluate the mechanical and moment impedances even when three dimensional elastic support materials have complex shape and physical property. Thus, when we calculate the vibration field of a plate with relatively complex supporting systems, we may split the calculation into two processes. In the preliminary step, the mechanical and moment impedances are determined by the problem as depicted in Fig. 5. Once the impedances are obtained, they can be input to the calculation geometry of which the supporting system is simplified as the impedance boundary.

Numerical modeling of the loss factor measurement was performed in order to investigate the difference between the theoretical and measured values. Compared with the theoretical TLF under the diffuse field assumption, the calculated values were overestimated due to the diffraction effect and the self-reverberation of the band pass filter. This tendency should be kept in mind when conducting inverse estimation of the support material's physical parameters or equivalent resistance, stiffness and inertance constants.

ACKNOWLEDGEMENTS

This project has been funded by a Grant-in-Aid for Young Scientists (B) from Japan Society for the Promotion of Science (No. 16K18196).

REFERENCES

[1] A. Berry, J. L. Guyader and J. Nocolas, "A general formulation for the sound radiation from rectangular baffled plate with arbitrary boundary conditions," *J. Acoust. Soc. Am.*, **88**, 2792–2802 (1990).

[2] T. Sakuma, K. Egawa and Y. Yasuda, "Numerical analysis of sound transmission loss of glass pane — On the treatment of edge damping," *Proc. Inter-Noise 2008*, No. 0486 (2008).

[3] A. W. Leissa, *Vibration of Plates* (Acoustical Society of America, New York, 1993).

[4] P. A. A. Laura and R. O. Grossi, "Transverse vibrations of rectangular plates with elastically restrained against translation and rotation," *J. Sound Vib.*, **75**, 101–107 (1981).

[5] G. B. Warburton and S. L. Edney, "Vibrations of rectangular plates with elastically restrained edges," *J. Sound Vib.*, **95**, 537–552 (1984).

[6] W. L. Li, "Vibration analysis of rectangular plates with general elastic boundary supports," *J. Sound Vib.*, **273**, 619–635 (2004).

[7] W. L. Li, X. Zhang, J. Du and Z. Liu, "An exact series solution for the transverse vibration of rectangular plates with general elastic boundary supports," *J. Sound Vib.*, **321**, 254–269 (2009).

[8] M. Heckl, "Measurements of absorption coefficients on plates," *J. Acoust. Soc. Am.*, **34**, 803–808 (1962).

[9] L. Cremer, M. Heckl and B. A. T. Petersson, *Structure-borne Sound*, 3rd ed. (Springer-Verlag, Berlin/Heidelberg, 2005).

[10] J. Yoshimura, S. Sugie and E. Toyoda, "Effects of size and edge damping on measurement results for sound reduction index of glass pane," *Proc. Inter-Noise 2006*, No. 641 (2006).

[11] T. Asakura and S. Sakamoto, "Study on the absorptive boundary condition of elastic plate in bending wave analysis," *Proc. Annu. Meet. Environ. Eng.* (Archit. Inst. Jpn.), pp. 233–234 (2008).